Acta Geophysica (2024) 72:2875–2885
https://doi.org/10.1007/s11600-023-01246-7

RESEARCH ARTICLE - ATMOSPHERIC & SPACE SCIENCES

Effect of excess ionospheric delay during six major geomagnetic storms on GPS positioning in Indian sector

Mohammed Yousuf[1,2] · Miriyala Sridhar[2] · Nirvikar Dashora[3]

Received: 5 February 2023 / Accepted: 9 November 2023 / Published online: 12 December 2023

Abstract

Some of the extreme space weather events like the geomagnetic storm of 17–18 March 2015 have produced dramatic effects on low-latitude ionosphere as reported in various studies. Similarly, some of the extreme storms are studied to emphasize the anomalous deviations in ionospheric delay; however, the effects of excess ionospheric delay on GPS-based positioning are rarely reported from India. This paper presents a robust analysis including estimation of GPS receiver position during 6 major geomagnetic storms using dual frequency GPS signals in L1 and L2 bands. Epoch-wise solution estimates are computed using precise orbit SP3 files for satellite orbit and clock corrections and receiver specific differential code biases are obtained from IGS-CODE center. A range domain Kalman filter has also been developed to smooth the 30 s sampled code pseudorange using carrier phase data and resolve the initial ambiguity. Then, the precise positioning residuals are estimated in two different cases of ionospheric corrected and ionospheric uncorrected error models. We then compare the results with ionospheric corrected position estimates to finally obtain the effect of excess daytime ionospheric variations during main phase of some extreme geomagnetic storms. Results from 5 GPS receivers located within 77°–80° E longitude sector are obtained for two 2-hour windows covering local noon during 6 storms including the St. Patrick's Day storm. The effect of severity of the storms and their impact on static precise positioning are brought out by comparing the results with performance on a quiet day. It is found that the magnitude of error in estimated altitude exhibits maximum deviations due to ionospheric variations during storms, and the dip latitude of station is important in terms of magnitude of ionospheric error in positioning over the equatorial ionization anomaly region.

Keywords Global positioning system · Positioning error · Kalman filter · Geomagnetic storms · Ionospheric delay · Equatorial and low latitudes

Introduction

The primary aim of GPS (global positioning system) is to provide accurate positioning, but the positioning is affected by major errors associated with satellites (clock and orbit errors), receivers (clock errors), atmosphere (neutral gases, water vapor and ionospheric electron density-related errors) and measurement noise and multipath (Kaplan 1996; Hofmann-Wellenhof et al. 2008). Using some of the advanced post processing techniques, these errors can be mitigated (see e.g. Dow et al. 2009; Dach et al. 2009; Kouba 2009; Zehentner and Mayer-Gürr 2016; Prange et al. 2017). These techniques include corrections of the atmospheric error, which is mostly referred to the ionospheric error and tropospheric error. The variations in the excess path delay due to ionosphere can be represented by the line-of-sight integral of the plasma density anywhere between the satellite, and the user receiver is referred as total electron content (TEC) or ionospheric delay (Klobuchar 1987). TEC can be estimated by a linear combination of the dual-frequency signal from a satellite (Hofmann-Wellenhof et al. 2008). Extremely variable nature of the ionospheric electron density in equatorial

Edited by Prof. Andrzej Krankowski (ASSOCIATE EDITOR) / Prof. Theodore Karacostas (CO-EDITOR-IN-CHIEF).

✉ Nirvikar Dashora
ndashora@narl.gov.in; nirvikardashora@gmail.com

[1] Vignana Bharathi Institute of Technology, Hyderabad 501301, India

[2] Department of ECE, Koneru Lakshmaiah Education Foundation, Guntur 522302, India

[3] National Atmospheric Research Laboratory, Gadanki 517112, India

and low latitudes creates highly heterogeneous and variable delay for a given user, and it impedes the accuracy of any delay forecast model (Shim et al. 2011; Li et al. 2015). It is significant to note that the single-frequency user receivers, who obtain their position estimates through the standard positioning service (SPS) technique, require a forecast model for real-time ionospheric corrections. Another major concern for the precise positioning techniques using single-frequency observables is the ionospheric divergence effect, which proves to be a hindering effect for using the carrier phase-based code smoothing algorithms (Kim et al. 2007; Park et al. 2017; Geng et al. 2019; Cui et al. 2023 and references therein). Recently, Wang et al. (2018) and Chen et al. (2018a) have compared ionospheric correction models using several combinations for SBAS as well as for un-differenced PPP (precise point positioning); however, there have been several issues when using any ionospheric model for equatorial and low latitudes (Shim et al. 2011). Standard ionospheric models like IRI (Bilitza 2018 and references therein) and NeQuick (Nava et al. 2011 and references therein) are also largely found to differ from real observations in low latitudes even during quiet geomagnetic durations (Venkatesh et al. 2014; Ezquer et al. 2018). Hence, further studies are highly needful to represent geomagnetic active periods and the correction of variable ionospheric error (Mengistu et al. 2018).

Extremely rapid variations in the low-latitude TEC are found to occur during space weather events (Suresh and Dashora 2016; Dashora et al. 2019). It is found that on occasions the ionospheric delay increases by more than 100% during main phase of the major geomagnetic storms (Mannucci et al. 2005; Suresh and Dashora 2016; Dashora et al. 2019), particularly within an interval of 2–6 h after the storm sudden commencement (SSC). Thus, during the major storms, spatial as well as temporal ionospheric gradients affect the standard positioning service (SPS) severely (Seeber 2003; Kintner and Ledvina 2005) due to un-corrected residuals. The variations in equatorial and low-latitude ionospheric delay during the storms are still a great threat to satellite-based navigation signals and have remained a challenge for forecasters (Doherty et al. 2002; Warnant et al. 2007; Skone 2001; Jacobsen and Schäfer 2012; Luo et al. 2018). Yousuf et al. (2023) have found that even the precise point positioning in the low latitudes shows different types of variabilities due to varying equatorial ionospheric conditions.

Hence, it is important to study the highly variable amount of the positioning error (which can also be referred to the un-corrected model errors) due to the extreme ionospheric conditions mentioned above. We use a Kalman-filter based technique to obtain smoothed carrier phase ranges and then estimate the positioning residuals in two different cases of ionospheric corrected and ionospheric uncorrected error models. We then compare the results with ionospheric corrected position estimates to finally obtain the effect of excess daytime ionospheric variations during main phase of some extreme geomagnetic storms. Further, we include more than one station to decipher the latitudinal variation in the error introduced by gradients in ionospheric delay over the equatorial ionization anomaly (EIA) region. Such studies have been very scant particularly from Indian low-latitude region. Hence, motivated by the effect of major storms and the resulting degradation in positioning, this study presents a comparative analysis of effect of some major geomagnetic storms of solar cycle 23 and 24. "Methodology and data" section gives the data and methods, "Results and discussion" section gives results and discussion and "Summary" section provides a summary of the results from this work.

Methodology and data

GPS-based positioning has evolved into several solutions like SPS, SPP (single point positioning), PPP (Bisnath and Gao 2009) in static and kinematic on the one hand, and absolute and differential schemes on the other hand. Each of these scheme addresses a particular set of applications (Dommety and Jain 1996; Peyret et al. 2000; Rizos 2003; Bisnath and Gao 2009; Gomez-Gil et al. 2013). As far as positioning using standalone GPS receiver is concerned, it can be solved using static SPS, static and kinematic SPP and PPP positioning methods (Luo 2013). All the methods also have inter-changeability through varying sets of algorithms and are detailed in several text books (Kaplan 1996; Rabbany 2002; Hofmann-Wellenhof et al. 2008) and review articles (Teunissen and Khodabandeh 2015). Particularly, the methods like SPP and PPP are immensely utilized in several applications that demand high precision, and these methods have further evolved into real-time kinematic solutions (Peyret et al. 2000; Lee et al. 2005; Lee and Rizos 2008; Zhao et al. 2009; Gomez-Gil et al. 2013; Chen et al. 2018b, 2019). Mostly these methods use the observations of pseudorange from code and carrier phase measurements at each epoch and obtain the positioning for locus of the receiver at each epoch of measurement with a few a-priori constraints and models for different errors. The basic aims of these algorithms are to fix the carrier phase ambiguity (Mervart et al. 2008; Wang et al. 2017) and minimize the errors in positioning using available set of measurements with statistically significant model of errors for a targeted accuracy. The fundamental GPS range equations can be given as below respectively for L1 and L2 signals -

$$P_i^j = \rho + \delta t_i * C - \delta t^j * C + T_p + I_p + M_p + \varepsilon^j, \quad (1)$$

$$\phi_i^j = \rho + \delta t_i * C - \delta t^j * C + T_p - I_p + M_p + \lambda * N_i^j + \in_\phi, \quad (2)$$

where ρ represents the true range of the satellite from the user receiver, whereas P_i^j represents pseudorange. Time of transmission by the satellite is given by t^j, and time of reception as determined by the receiver is t_i. Difference of these two epochs from the GPS time is δt^j known as satellite clock correction and δt_i as receiver clock correction. Here, τ_i and τ^j refer to common time system, where $\Delta t = \tau_i - \tau^j$ and $\Delta\delta = \delta t_i - \delta t^j$. The bias δt^j of the satellite clock can be modeled using coefficients transmitted in the navigation message. The correction δt^j converts $\Delta\delta$ into the receiver clock bias. $\in_\phi$ represent un-modeled error with white noise characteristics. I_p, T_p, M_p, N_i^j and λ respectively represent ionospheric delay, tropospheric delay, multipath error, integer ambiguity and wavelength of the carrier signal (L1 at ~ 19 cm and L2 at ~ 24 cm). Integer ambiguity additively affect the carrier phase measurements making them highly relative, whereas the code pseudorange measurements suffer from inherent higher noise due to bit-resolution of the code (i.e., C/A or P-code) on respective signals. The precise positioning takes advantage of precise carrier phase measurements, known and accurate satellite orbits and clock using SP3 products (Kouba and Héroux 2001) of IGS (international GNSS service) as well as estimated atmospheric delays. However, SPS takes the navigation message into account for model corrections of the errors using broadcast orbits. We aim carrier phase ambiguity resolution (Mervart et al. 2008) through carrier smoothed code range technique. A Kalman filter-based code-smoothing is performed for each signal measurement as described below.

Range domain Kalman filter and positioning

The initial ambiguity in the carrier phase pseudorange remains constant for a given pass of a satellite over a GPS site as long as there is no cycle slip (Blewitt 1990) recorded in the data. Thus, to utilize the precise phase measurements, absolute code measurements are smoothed using the relative carrier phase. Hatch filter (Hatch 1982) has been customarily used algorithm for such purposes, however, due to its initial convergence time and dependence on length of continuous data set a Kalman filter is preferred. Kalman filter (Kalman 1960) has found immense applications in GPS-based data processing (King and Bock 2009; Herring et al. 2015; Mazher et al. 2016) owing to its fast convergence and robust control on Kalman gain for the prediction of future state of the system with recursive feedback. For the present study, a range domain Kalman filter (KF)-based technique has been developed using following framework:

$$\hat{x}_k^- = \Phi_{k-1}\hat{x}_{k-1}^+, \tag{3}$$

$$P_k^- = \Phi_{k-1}P_{k-1}^+\Phi_{k-1}^{\mathrm{T}} + Q_{k-1}. \tag{4}$$

The error covariance of the true measurement vector is:

$$E\left(\left(z_k - H_k x_k\right)\left(z_k - H_k x_k\right)^{\mathrm{T}}\right) = R_k, \tag{5}$$

$$\text{Kalman Gain:} K_k = P_k^- H_k^{\mathrm{T}}\left(H_k P_k^- H_k^{\mathrm{T}} + R_k\right)^{-1}. \tag{6}$$

$$\text{Measurement update}: \hat{x}_k^+ = \hat{x}_k^- + K_k\left(z_k - H_k\hat{x}_k^-\right). \tag{7}$$

$$\text{Error Covariance update:}\ P_k^+ = \left(I - K_k H_k\right)P_k^-, \tag{8}$$

where the symbols represent state transition matrix, Φ_{k-1}, system noise covariance matrix, Q_{k-1}, state vector estimate future state and previous state, $\hat{x}_{k-1}^+$ to $\hat{x}_k^-$, error covariance matrix for future and past states P_{k-1}^+ to P_k^-, measurement matrix,H_k, measurement noise covariance matrix, R_k, and Kalman gain matrix,K_k. carrier phase measurements are used to estimate the error covariance (R_k) and that is later used in estimation of Kalman gain (K_k).

The above-mentioned Eqs. (3–5) are used for smoothing code pseudorange using the carrier phase pseudorange measurements. Equations 3 and 4 are time update equations used along with previous updates. The later Eqs. (6–8) are measurement update equations. Initially, we calculate the epoch-wise difference of carrier phase, which is then added to a previous epoch used as a posteriori to get a priori estimate, then the predicted covariance (P_k^-) is calculated using the updated covariance of previous epoch by adding the system noise covariance (Q_{k-1}) following Eq. 4. Carrier phase measurements are used to estimate the error covariance (R_k) and that is later used in estimation of Kalman gain (K_k) following Eqs. 5 and 6. The carrier phase measurement updates are obtained using Eq. 7 and the Error covariance is updated using predicted covariance (P_k^-) following Eq. 8.

Previous studies have used the KF in position estimation domain as well as in range domain (Hatch 1982; Lee et al. 2005; Chen et al. 2018b). The range domain KF has been customarily used with phase measurements of very high rate data (e.g., 1 s or lower sampling interval) (Mazher et al. 2016); however, in the present analysis, KF is used for 30-s sampling data. A geomagnetic quiet day is selected to test the performance of the range domain KF on high rate as well as 30-s sampled data. Carrier phase measurements (without cycle slip) are used to estimate the true error covariance (P) that updates the Kalman gain from one epoch to another. It is found that system noise covariance (Q) and initial value of updated error covariance need to be optimized for desired level of smoothing, wherein the initial value of the former has been set at 0.5 and later at 1.0 to obtain the results shown in Figs. 1 and 2. Figure 1 shows the performance of the above mentioned framework of KF for high rate data recorded using a software GNSS receiver (IFEN-GmbH

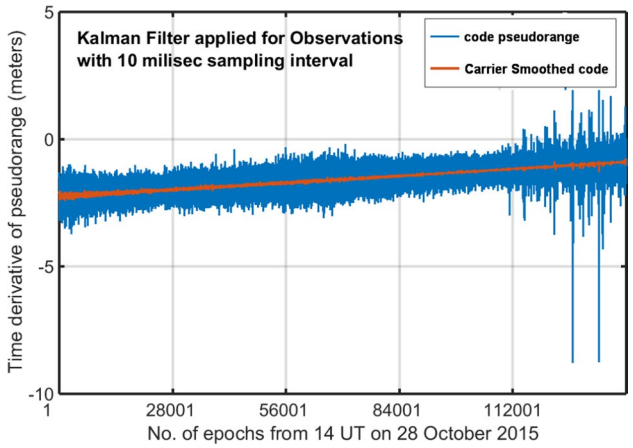

Fig. 1 Kalman filter-based smoothing of high rate sampled code pseudorange using L1C code and L1 carrier phase as observed from NARL, Gadanki station on 28 October 2015 using IFEN make SX-NSR software receiver

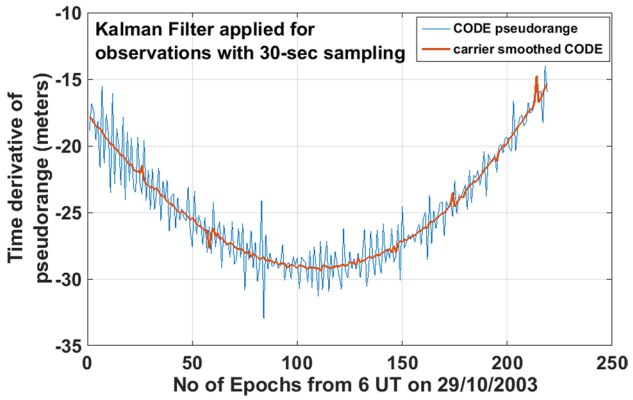

Fig. 2 Kalman filter-based smoothing of 30-s sampled code pseudorange using L1C code and L1 carrier phase as observed from IISC, Bangalore station, on 29 October 2003

make SX-NSR receiver) operational at NARL, Gadanki, India (13.4593° N, 79.177° E), on 28 October 2015. High rate (10 ms sampling interval) data of 35-min duration for PRN 11 for both the code and carrier phase are used as input to the KF, and output is shown in terms of the first time derivative of the original code pseudorange (blue curve) and of the KF-based smoothed code pseudorange (red curve) in Fig. 1. The performance of smoothing using same KF over 30-s sampled code pseudorange and carrier phase measurements as observed from IISC, Bangalore station, on 29 October 2003. It is found that a set of initial P and Q values can be obtained for a given site that mostly remains same for different days. It can be seen from Fig. 1 that the temporal fluctuations in code pseudorange remain within 2 m while using high rate data and the same reduces to a few cm after smoothing, whereas it is evident that the noise in code pseudorange remains higher for sampling interval of 30-s as seen in Fig. 2; however, performance of the KF gives the desired level of smoothing. Some spikes in the smoothed code are visible, but they do not correspond to spikes in the code pseudorange and it could be due to process noise or due to P and Q updates.

Figure 2 shows double time derivative for 30-s sampled data. The double derivative is needed because the change in ranges becomes too large to showcase the smoothing, which is at order of a meter. Test of this KF with 30-s sampled data shows satisfactory performance as examined using different data sets and sites; however, the smoothing after 120 min of data shows divergence in code and carrier measurements due to the parameterization of the KF. The cumulative ionospheric error produces the code to carrier phase divergence on the same frequency (say L1) and several previous studies (see Cui et al. and references therein) have come-across such divergence-related issues using the Hatch filter. For example, Kim et al. (2007) have shown an optimal carrier smoothing method by taking a recursive estimation of the divergence. There are many studies, which highlight the divergence issue in different experimental set-ups, like Park et al. (2017) have proposed an optimal single-frequency (SF) divergence-free Hatch filter that uses a satellite-based augmentation system (SBAS) message to reduce the ionospheric divergence. Similarly, Geng et al. (2019) have used another improved hatch filter with three thresholds and single divergence Hatch filter for Android-based low-cost single-frequency GNSS receivers. In present study, the optimization of the divergence is limited by the filter window of 2-h, so that the accuracy of the KF technique is not compromised. Figure 3 shows an example selected to showcase the comparative variations in positioning error for “Latitude” coordinate on 18 March 2015. Figure 3 shows the variations of the "iono-corrected," "uncorrected" and the IGS reference value of the "Latitude" coordinate during a 2-hour window (6–8 UT) on the second day of the St. Patrick’s Day storm on 18 March 2015. Thus, the results of this study are limited to 2-h continuous time window from each site at a given day, and KF parameters are reset after every 2 h. This provides us with smooth, unambiguous and precise pseudoranges that can be directly applied for estimation of position using least squares (He and Bilgic 2011; Tian et al. 2013; Das and Nakamura 2016). The epoch-wise precise position estimates in terms of latitude, longitude and altitude are obtained for each 30-s interval in two different cases one in the dual-frequency ionosphere-free combination (called as “iono-corrected”), and other the smoothed ranges (called as “iono-uncorrected”). In both the cases, all other errors are corrected so as to compare the effect of only “ionospheric error” on positioning. The precise satellite orbit and clocks corrections are employed using precise GPS orbits downloaded in SP3 format from ftp://igs.org/pub/gps and the RINEX observation files are

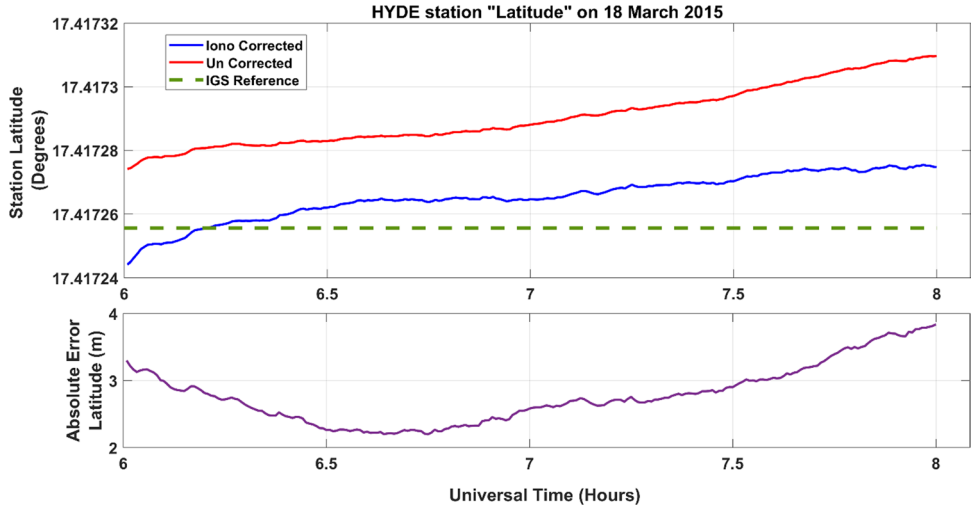

Fig. 3 Variations in the estimated positioning for "Latitude" coordinate without applying ionospheric corrections (called as "Uncorrected"—red curve) and after applying ionospheric corrections (called as "Iono Corrected"—blue curve) in comparison to the IGS reference position (dashed Green) of HYDE receiver, are given in the top panel. The bottom panel shows the variations in the absolute error in the "iono-corrected" estimate of the "Latitude" with reference to the IGS value for a 2-hour window (6–8 UT) during the second day of the St. Patrick's Day storm on 18 March 2015

downloaded from http://sopac.ucsd.edu/dataBrowser.shtml for the concerned durations and sites given below. The ionospheric delay is estimated using dual frequency carrier phase measurements from the observations following Dashora et al. (2012) and the differential code biases (DCBs) are corrected using corresponding DCB files obtained from IGS analysis from ftp://ftp.aiub.unibe.ch/CODE/. DCBs for the NARL (National Atmospheric Research Laboratory) network of stations are estimated using the minimum scalloping technique of Arikan et al. (2008) for zero-difference TEC variability. The clock and other errors like satellite and receiver specific DCBs are corrected from ranges and tropospheric delay has been taken from the model (Hopfield 1972; Herring et al. 2015). The receiver position is estimated at every time epoch using all the corrected smoothed ranges minimizing the remaining errors in a general least square sense that is similar to the standard method used in the most kinematic algorithms. It shall be noted that the aim of this study is to showcase the first-order ionospheric effects on positioning and hence, ionosphere-free combination justifies the use even though it is known to enhance errors in range domain positioning (GPS-SPS 2008; Lee and Rizos 2008; Banville et al. 2017; Chen et al. 2018b) which may not exceed a few centimeters.

Observations sites, storms events and data durations

GPS stations are selected from low latitudes covering the EIA crest region and temperate latitudes in Indian sector. Table 1 provides the list of the major storms selected under this study along with respective sites, site name codes and duration of data that is analyzed for each storm. Observations from IGS network stations (1) Hyderabad (17.4166° N, 78.5508° E) (3) Bangalore (13.021° N, 77.5703° E) are used for all the storms. Additionally, for the storm of 17 March 2015, observations from (3) Lucknow (26.9121° N, 80.955° E) (4) Vignana Bharathi Institute of Technology (VBIT) (17.4705° N, 78.7211° E) and (5) NARL (13.4593° N, 79.177° E) stations have been used to emphasize upon the latitudinal and longitudinal differences due to ionospheric variations. The scintillation monitoring GPS receivers at NARL and VBIT are installed by NARL, Gadanki under a project, network of GNSS receivers in India. The position estimates on a quiet day prior to the storm are taken as a reference to decipher the effect of the geomagnetic storms. Dual-frequency L1 and L2 GPS raw observations from each station are used for this study. Total 6 major ionospheric storms (minimum Dst < – 200 nT) have been selected based upon the occurrence of main phase of the storms in daytime over Indian sector. The impact of geomagnetic storm is known to be highest near the crests of EIA (Suresh and Dashora 2016) than anywhere on the globe so observations covering anomaly zone latitude from Indian sector are included in the analysis. Positioning is obtained under each storm for 2 hourly durations to cover the effect of PPEF. To avoid sudden variations in position due to GDOP, only those PRNs are chosen that were continuously available in the 2 hourly windows and have continuous carrier phase measurements without cycle slips. The estimates are primarily performed as residual in the three coordinates (altitude, latitude and longitude), however, for a comparison with other

Table 1 A list of major storms analyzed under this study along with corresponding set of GPS stations and data durations used to estimate position

S. no.	Storm	GPS station (IGS-NAME)	2-h duration (UT) for positioning
1	29 and 30 October 2003	HYDE	6–8, 8–10
		IISC	6–8, 8–10
2	20 November 2003	HYDE	6–8, 8–10, 10–12, 12–14
		IISC	6–8, 10–12, 12–14
3	09 November 2004	HYDE	6–8, 8–10
		IISC	6–8, 8–10
4	15 May 2005	HYDE	6–8,8–10
		IISC	No data
5	24 August 2005	HYDE	6–8, 8–10, 10–12
		IISC	6–8, 8–10, 10–12
6	17 and 18 March 2015	HYDE	6–8, 8–10, 14–15, 16–18
		IISC	6–8, 8–10
		LCK3	6–8, 8–10
		VBIT	6–8, 8–10
		NARL	6–8, 8–10

studies, finally results in Tables 2, 3 and 4 are given in horizontal and vertical error. Most of the single point positioning methods based upon stand-alone dual-frequency observations suggest for 2–4 h' duration of the window for precise positioning (Zhao et al. 2009; Ahmed and Ayman 2013).

Results and discussion

The emphasis of this study is to showcase the effects of ionospheric variability during storms on standard positioning using GPS observations. The magnitude of ionospheric error in terms of final position estimates are tabulated for various intensities of storms. As noted in Table 1, positioning analysis is performed for 6 major storms and, data from 2 stations HYDE and IISC for all the storms and data from 3 more stations LCK4, VBIT and NARL only for the storm of St Patrick's day have been analyzed (depending upon the availability). Results for each time window under "iono-corrected" and "iono-uncorrected" cases are prepared for all the durations, and RMS difference between the two cases is calculated for all the storms.

Similar analysis has been performed for all the cases for all the 6 major storms for 2-hourly windows as well as for 3 sample cases of quiet days using 4 stations. The results are computed in terms of RMS difference for each window and given in Tables 2, 3 and 4. Table 2 shows results for analysis performed for quiet days. Table 3 shows the results for HYDE and IISC station for all the storm for altitude, latitude and longitude estimates, whereas, Table 4 has specifically been prepared to show the results from all 5 stations for the storm of St. Patrick's Day on 17 and 18 March 2015. Quiet time estimate of the RMS differences is shown in Fig. 4 for HYDE (cyan) and IISC (brown) stations for 6–8 UT and 8–10 UT, respectively. It is found that the RMS difference of IISC altitude remains mostly equal to that of

Table 2 RMS differences (in meters) between iono-corrected and iono-uncorrected estimate for 3 quite days are shown in table above

S. no.	HYDE		IISC		VBIT		NARL	
	6–8 UT	8–10 UT	6–8 UT	8–10 UT	6–8 UT	8–10 UT	6–8 UT	8–10 UT
Vertical (m)								
11-10-2003	11.28	10.49	11.32	8.51	-NA-	-NA-	-NA-	-NA-
06-11-2004	6.72	9.96	9.44	9.81	-NA-	-NA-	-NA-	-NA-
16-03-2015	11.39	12.25	14.66	5.02	7.82	12.66	7.29	15.03
Horizontal (m)								
11-10-2003	2.28	4.80	1.36	0.92	-NA-	-NA-	-NA-	-NA-
06-11-2004	1.59	0.72	0.68	0.98	-NA-	-NA-	-NA-	-NA-
16-03-2015	2.22	4.12	4.21	2.22	2.25	2.10	1.47	3.59

The top rows show the IGS station code names of the stations along with respective 2 h windows and the left column shows quiet day. RMS difference is shown for vertical and horizontal differences

Table 3 RMS differences of geomagnetic storm days other than St. Patrick's day storm

Storm days	HYDE		IISC	
	6–8 UT	8–10 UT	6–8 UT	8–10 UT
Vertical (m)				
29-10-2003	10.21	18.57	26.49	18.04
30-10-2003	6.99	11.50	9.02	10.88
20-11-2003	7.45	10.54	10.78	NO DATA
09-11-2004	12.54	11.53	14.84	12.13
15-05-2005	5.052	5.69	No data	No data
24-08-2005	7.38	4.43	5.91	5.88
Horizontal (m)				
29-10-2003	2.54	3.54	4.64	1.89
30-10-2003	0.80	1.40	2.23	0.95
20-11-2003	0.97	1.49	0.64	No data
09-11-2004	1.45	1.52	0.70	0.51
15-05-2005	0.32	1.43	No data	No data
24-08-2005	1.17	0.52	0.89	0.54

The above table shows the different severe geomagnetic storms that occur in Solar Cycle 23 and 24. The top panel of the table represents RMS in terms of vertical error for both the stations (Hyderabad and Bangalore) during the selected time period, i.e., (6–8) UT and (8–10) UT. Similarly, the bottom panel shows RMS of the horizontal error

HYDE (~ 10–12 m) during 8–10 UT but grows higher than HYDE during 6–8 UT. In case of RMS differences for latitude and longitude, the values of HYDE (~ 3–5 m) mostly remain higher than IISC (~ 1–3 m) except during 6–8 UT on 16 March 2015.

In comparison to the quiet days, the RMS difference of altitude on storm days grows substantially higher over IISC (~ 15–25 m) than over HYDE (~ 10–15 m) preferably during 6–8 UT than 8–10 UT. Maximum RMS is found during the Halloween storm of 29 October 2003. It is found that RMS differences on storm of 09 November 2004 remained lowest among the three storms for all the three coordinates. RMS difference of latitude shows storm dependent variations albeit with higher effect over IISC then over HYDE, whereas inverse is true in case of RMS difference of longitude. The obvious changes have been observed between IISC and HYDE for each time window and each storm, indicating variable ionospheric effects in low latitudes. Also, a direct comparison between Figs. 4 and 5 provides a clear impact of excess ionospheric delay that has enhanced the RMS differences for each coordinate due to ongoing ionospheric storms. Bergeot et al. (2011) have emphasized the impact of this storm on GPS-based kinematic positioning using high-resolution ionospheric delay over mid latitudes. However, our study is aimed on effect of excess ionospheric delay on static (un-differenced) positioning over equatorial and low latitudes. It shall be mentioned that the PPEF associated with high-latitude convection increases the total vertical ExB drift of low-latitude F-region and thus, ionospheric TEC increases drastically during daytime (Dashora et al. 2009; Suresh and Dashora 2016). The steep gradients formed due to response of low-latitude ionosphere to PPEF in the EIA region produce enhanced line of sight ionospheric delay that, if left uncorrected, result into degraded position as seen from Figs. 4 and 5.

Table 2 provides the results of analysis performed for 3 quiet days over 4 stations. The RMS differences vary between ~ 5–15 m for vertical and ~ 0.6–5 m for horizontal errors and show the high noon-time variability of low latitude. Table 3 shows the same for 6 storm days over HYDE and IISC stations. The results of 3 storms is shown in Fig. 5; however, the variations of RMS during other storms in Table 3 show a strong dependence on severity of the storms. It is clearly seen that the variations in RMS of vertical error grows higher than the horizontal coordinates by almost 6–10 m. This result is in conformity with previous studies of Luo et al. (2018) and references therein that the solutions for altitude under precise positioning are biased. Coming to the error in the horizontal coordinates, the RMS remains less than 1 m for all the storms, except the storm of 29 October 2003, during both the time windows and sometimes remains lesser than the variation in RMS on quiet days. While high RMS corresponds to excess

Table 4 The RMS difference during the St. Patrick's day geomagnetic storm that occurred on 17–18, March 2015 is shown from five stations

Name of the station	17 Mar 2015				18 Mar 2015			
	6–8 UT		8–10 UT		6–8 UT		8–10 UT	
	Vertical	Horizontal	Vertical	Horizontal	Vertical	Horizontal	Vertical	Horizontal
HYDE	12.75	1.36	11.66	3.27	7.61	2.03	12.64	1.84
IISC	17.63	5.56	11.08	2.54	17.97	4.61	17.71	3.88
LCK4	10.18	4.11	13.24	3.33	12.93	4.83	13.01	3.18
VBIT	12.55	1.57	15.71	2.84	10.35	2.24	12.33	1.77
NARL	10.59	1.24	15.39	3.19	7.63	1.93	13.52	1.93

Different stations are shown in first column and corresponding vertical and horizontal RMS values are shown for the selected time slot of 6–8 UT and 8–10 UT according to the row of the station, respectively for 17 and 18 March in different columnar panels

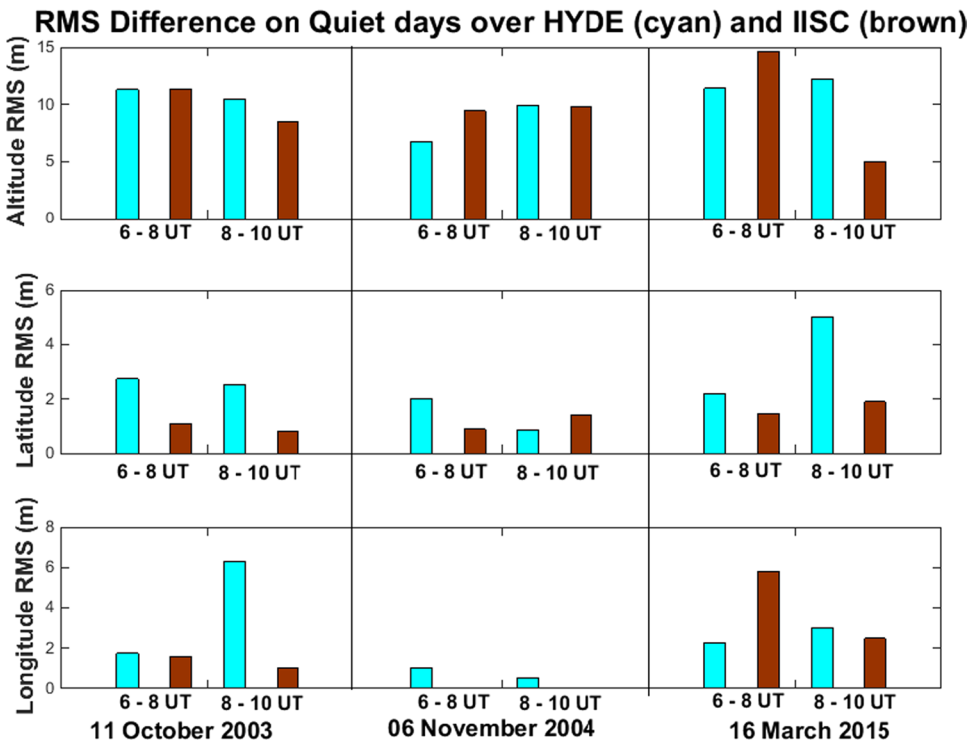

Fig. 4 RMS difference of iono-corrected and uncorrected solutions of altitude (top), latitude (middle) and longitude (bottom) estimated on sample quiet days in month of October 2003 (left), November 2004 (middle) and March 2015 (right). Bars show the RMS for 2 time windows under each case, respectively for 6–8 UT and 8–10 UT, over HYDE (cyan color) and IISC (brown color) stations

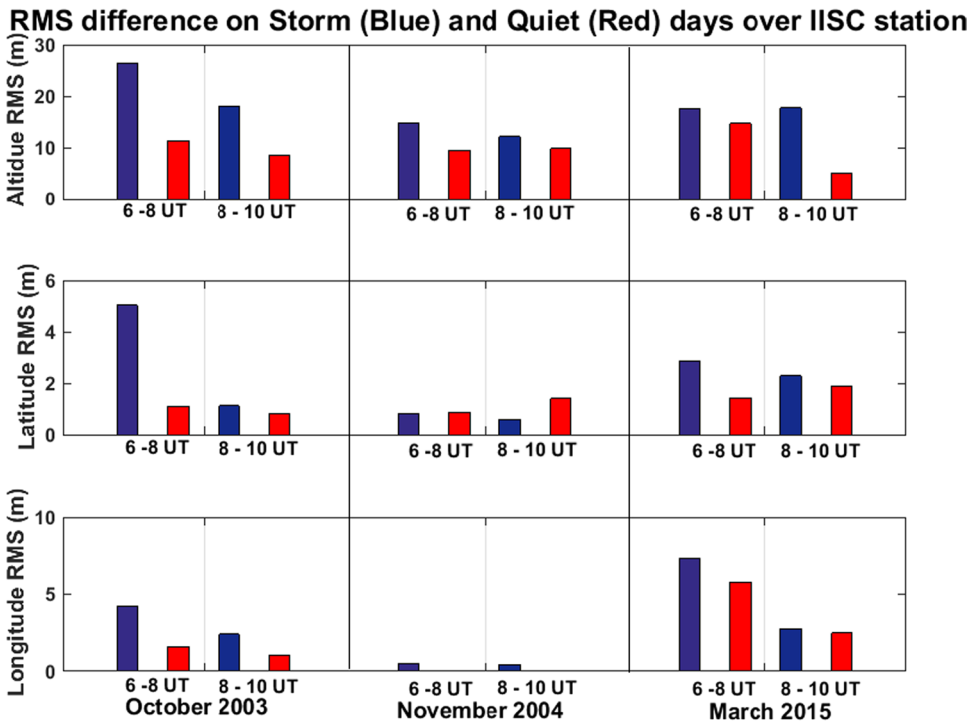

Fig. 5 RMS difference on storm day (blue) and Quite day (red) for IISC station

ionospheric delay during daytime, the low RMS during storms may indicate presence of negative storm. Suresh and Dashora (2016) have emphasized on occurrences of positive and negative ionospheric storms wherein, a positive (negative) storm was defined by enhanced (decreased) ionospheric delay beyond the day-to-day variability over a latitude and time interval. Also, Dashora et al. (2019) and Kader et al. (2022) have corroborated the effect of the westward PPEF during daytime for the occurrence of a negative ionospheric storm during main phase of the respective storms, which explains the observed decrease in the RMS for some cases of storms compared with quiet

days. Since the position estimates are obtained as independent solution for each epoch for the 2-hourly window for each case, and RMS is obtained as single value for this duration, the low RMS on some storm days compared with quiet day possibly represent the cases of negative daytime effect of the PPEF.

Since this study is majorly motivated by the storm of 17–18 March 2015, data from 5 stations has separately been analyzed for both the stormy days, and the results are given in Table 4. When comparing the RMS differences of the vertical coordinate between 6–8 UT and 8–10 UT on 17 March 2015, it is found that most of the stations exhibit higher values in a later time window on the day of the storm. The RMS of the horizontal coordinates remains mostly lower during 6–8 UT and shows mixed response for other stations with overall marginal changes of about 1 m for all the stations. When comparing the similar time windows between 17 and 18 March, it is found that RMS of the vertical coordinate during 6–8 UT mostly remained higher on 18 March than 17 March but RMS of horizontal coordinate has mostly increased. Similarly, the RMS of the vertical coordinate during 8–10 UT has mostly increased on 18 March and that of the horizontal coordinate decreased compared to 17 March. Coming to the comparison of RMS difference with regard to the horizontal error of stations, it is found that mostly the peak RMS is obtained in both the windows for LCK4 station, which is located under the crest of EIA in Indian sector followed by the RMS over IISC, and the other stations show mostly similar values of RMS. It is surprising that the RMS difference of altitude over IISC station has peaked in both the time windows followed by HYDE/VBIT, LCK4/NARL.

It is well known that the temporal variations of ionospheric slant delay are further complicated by latitudinal variation of delay due to presence of EIA in equatorial and low latitudes. There have been several reports emphasizing sudden effects of PPEF on ionospheric electron density during daytime (Dashora et al. 2009; Astafyeva et al. 2015; Dashora et al. 2019) which are mostly short lived. Thus, it is possible that the during an ongoing storm, two consecutive time intervals of 2 h respond drastically differently in terms of total ionospheric delay during daytime. Further, the position is function of slant ionospheric delay, which includes horizontal gradients in the EIA region. So, for a given time epoch, computation of position depends upon the set of satellites being used in the solution. The effect of dip latitude of a station on estimated position also depends upon how that particular set of satellites cuts-across the different gradients of ionosphere. This explains the effect of ionospheric variations on final position estimate and the RMS difference between iono-corrected and iono-uncorrected estimates around noon time during various storms.

Summary

1. A range domain Kalman filter is developed to obtain smoothed code pseudorange based upon carrier phase ranges using 30-s sampling interval. The performance of this new KF is validated using data from 5 stations located in the Indian low-latitude sector. This is used to resolve the initial ambiguity of carrier phase measurements for each 2-hourly time window.
2. Precise position of each station is estimated by applying epoch wise smoothed ranges, precise satellite orbits and clock corrections, satellite and receiver DCBs in (1) ionosphere-corrected and (2) ionosphere-uncorrected modes in a relative sense. RMS difference between "iono-corrected" and "iono-uncorrected" estimate of altitude, latitude and longitude is considered to emphasize the effects of excess daytime ionospheric delays during storms.
3. Six major storms are selected that occurred during daytime in the Indian sector, and the positions estimated during storm day are compared with quiet day estimates from 5 different stations over the Indian low-latitude region.
4. This study is probably the first such attempt from the Indian sector to quantify the effect of extreme storm time ionospheric variation of GPS positioning. A robust statistical analysis has been carried out to establish the differences.
5. Main results show that the severity of a geomagnetic storm relates with the magnitude of the error in estimated coordinates and estimated altitude exhibit maximum deviations due to ionospheric variations. Also, the dip latitude of a station is important in terms of the magnitude of the excess ionospheric error in positioning over the EIA region.

Acknowledgements Installation of a GPS/GNSS receiver at VBIT (Vignana Bharati Institute of Technology), Hyderabad, is performed by the National Atmospheric Research laboratory (NARL), Department of Space, Government of India, under a project of chain of GNSS receivers. One of the authors, MY is thankful for the research fellowship granted by the ISRO under RESPOND [No.ISRO/RES/2/406/16-17] program and to the Director, NARL, for his support during this collaborative study.

Funding This study was partially funded by the Indian Space Research Organization (ISRO) under RESPOND (No. ISRO/RES/2/406/16-17) program. The study is supported by Department of Space, Government of India under a project of GNSS network at NARL.

Declarations

Conflict of interest On behalf of all authors, the corresponding author states that there is no conflict of interest.

References

Ahmed ER, Ayman FR (2013) Enhancement of GPS single point positioning accuracy using referenced network stations. World Appl Sci J 18(10):1463–1474

Arikan F, Nayir H, Sezen U, Arikan O (2008) Estimation of single station interfrequency receiver bias using GPS-TEC. Radio Sci 43:RS4004. https://doi.org/10.1029/2007RS003785

Astafyeva E, Zakharenkova I, Förster M (2015) Ionospheric response to the 2015 St. Patrick's Day storm: a global multi-instrumental overview. J Geophys Res Space Phys 120:9023–9037. https://doi.org/10.1002/2015JA021629

Banville S, Sieradzki R, Hoque M (2017) On the estimation of higher-order ionospheric effects in precise point positioning. GPS Solut 21:1817. https://doi.org/10.1007/s10291-017-0655-0

Bergeot N et al (2011) Impact of the Halloween 2003 ionospheric storm on kinematic GPS positioning in Europe. GPS Solut 15:171–180

Bilitza D (2018) IRI the international standard for the ionosphere. Adv Radio Sci 16:1–11. https://doi.org/10.5194/ars-16-1-2018

Bisnath S, Gao Y (2009) Precise point positioning: a powerful technique with a promising future. GPS World 20(4):43–50

Blewitt G (1990) An automatic editing algorithm for GPS data. Geophys Res Lett 17(3):199–202. https://doi.org/10.1029/GL017i003p00199

Chen L, Yi W, Song W et al (2018a) Evaluation of three ionospheric delay computation methods for ground-based GNSS receivers. GPS Solut 22:125. https://doi.org/10.1007/s10291-018-0788-9

Chen C, Chang G, Zhang S, Chen G, Luo F (2018b) New range domain carrier-smoothed code filtering with dual-frequency BDS data. Asian J Control. https://doi.org/10.1002/asjc.1996

Chen C, Chang G, Luo F, Zhang S (2019) Dual-frequency carrier smoothed code filtering with dynamical ionospheric delay modeling. Adv Space Res 63(2):857–870. https://doi.org/10.1016/j.asr.2018.10.004

Cui H, Zhang S, Li J (2023) An improved phase-smoothed-code algorithm using GNSS dual-frequency carrier epoch-difference geometry-free combination observations. Adv Space Res 71(8):3433–3443

Dach R, Brockmann E, Schaer S, Beutler G, Meindl M, Prange L, Bock H, Jäggi A, Ostini L (2009) GNSS processing at CODE: status report. J Geodesy 83(3–4):353–365. https://doi.org/10.1007/s00190-008-0281-2

Das PP, Nakamura S (2016) Analysis of GPS single point positioning and software development. Int J Electron Commun Technol 7(1)

Dashora N, Sharma S, Dabas RS, Alex S, Pandey R (2009) Large enhancements in low latitude total electron content during 15 May 2005 geomagnetic storm in Indian zone. Ann Geophys 27:1803–1820. https://doi.org/10.5194/angeo-27-1803-2009

Dashora N, Taori A, Patra AK (2012) Multi instrument observations of winter solstice F-region irregularities during the low solar activity. Indian J Radio Space Phys 41:220–232

Dashora N, Suresh S, Niranjan K (2019) Interhemispheric asymmetry in response of low-latitude ionosphere to perturbation electric fields in the main phase of geomagnetic storms. J Geophys Res Space Phys 124(8):7256–7282. https://doi.org/10.1029/2019JA026671

Doherty PH, Dehel T, Klobuchar JA, Delay SH, Datta-Barua S, de Paula ER, Rodrigues FS (2002) Ionospheric effects on low-latitude space based augmentation systems. In: Proceedings of ION GPS 2002. September 24–27. Portland, 1321–1329, Oregon

Dommety G, Jain R (1996) Potential networking applications of global positioning systems (GPS). Technical report TR-24, The Ohio State University

Dow JM, Neilan RE, Rizos C (2009) The international GNSS service in a changing landscape of global navigation satellite systems. J Geodesy 83(3–4):191–198. https://doi.org/10.1007/s00190-008-0300-3

Ezquer RG, Scidá LA, Migoya Orué Y, Nava B, Cabrera MA, Brunini C (2018) NeQuick 2 and IRI Plas VTEC predictions for low latitude and South American sector. Adv Space Res 61(7):1803–1818. https://doi.org/10.1016/j.asr.2017.10.003

Geng J, Jiang E, Li G, Xin S, Wei N (2019) An improved Hatch filter algorithm towards sub-meter positioning using only Android raw GNSS measurements without external augmentation corrections. Remote Sens 11(14):1679

Gomez-Gil J, Ruiz-Gonzalez R, Alonso-Garcia S, Gomez-Gil FJ (2013) A Kalman filter implementation for precision improvement in low-cost GPS positioning of tractors. Sensors (basel, Switzerland) 13(11):15307–15323. https://doi.org/10.3390/s131115307

GPS-SPS (2008) GPS standard positioning service (SPS) specifications. http://www.gps.gov/technical/ps/2008-SPS-performance-standard.pdf. Accessed 01 Feb 2023

Hatch R (1982) The synergism of GPS code and carrier measurements. In: Proceedings of 3rd int. geodetic symposium on satellite doppler positioning. 2 New Mexico State University, 8–12 February 1982, pp 1213–1231

He Y, Bilgic A (2011) Iterative least squares method for global positioning system. Adv Radio Sci 9:203–208. https://doi.org/10.5194/ars-9-203-2011

Herring TA, King RW, Floyd MA, McClusky SC (2015) Introduction to GAMIT/GLOBK. Release 10:6

Hofmann-Wellenhof B, Lichtenegger H, Wasle E (2008) GNSS—global navigation satellite systems: GPS, GLONASS, Galileo, and more. Springer, Vienna, Austria. https://doi.org/10.1007/978-3-211-73017-1 (**978-3-211-73012-6**)

Hopfield HS (1972) Tropospheric range error at the zenith. Space Research XII, Akademie-Verlag, Berlin

Jacobsen KS, Schäfer S (2012) Observed effects of a geomagnetic storm on an RTK positioning network at high latitudes. J Space Weather Space Clim 2:A13

Kader SS, Dashora N, Niranjan K (2022) Spatial and temporal confinement of the ionospheric responses during the St. Patrick's Day storm of March 2015. Space Weather 20(9):157. https://doi.org/10.1029/2022SW003157

Kalman RE (1960) A new approach to linear filtering and prediction problems. Trans ASME J Basic Eng 82:35–45

Kaplan ED (1996) Understanding GPS: principles and applications. Artech House, Norwood

Kim E, Walter T, Powell JD (2007) Adaptive carrier smoothing using code and carrier divergence. In: Proceedings of the 2007 national technical meeting of the institute of navigation, pp 141–152

King R, Bock Y (2009) Documentation for the GAMIT GPS analysis software. Release 10:2

Kintner PM, Ledvina BM (2005) The ionosphere, radio navigation, and global navigation satellite systems. Adv Space Res 35(5):788–811. https://doi.org/10.1016/j.asr.2004.12.076

Klobuchar J (1987) Ionospheric time-delay algorithms for single-frequency GPS users. IEEE Trans Aerosp Electron Syst 3:325–331

Kouba J (2009) A guide to using international GNSS service (IGS) Products. acc.igs.org/UsingIGSProductsVer21.pdf. Accessed 04 Mar 2019

Kouba J, Héroux P (2001) Precise point positioning using IGS orbit and clock products. GPS Solut 5:12. https://doi.org/10.1007/PL00012883

Lee HK, Rizos C (2008) Position-domain Hatch filter for kinematic differential GPS/GNSS. IEEE Trans Aerosp Electron Syst 44(1):30–40. https://doi.org/10.1109/TAES.2008.4516987

Lee HK, Rizos C, Jee GI (2005) Position domain filtering and range domain filtering for carrier-smoothed-code DGNSS: an analytical comparison. IEE Proc Radar Sonar Navig. https://doi.org/10.1049/ip-rsn:20059008

Li X, Zhang X, Ren X, Fritsche M, Wickert J, Schuh H (2015) Precise positioning with current multi-constellation Global Navigation Satellite Systems: GPS, GLONASS. Galileo and BeiDou. Sci Rep 5:8328. https://doi.org/10.1038/srep08328

Luo X (2013) Mathematical models for GPS positioning. In: GPS Stochastic modelling, Springer theses (recognizing outstanding Ph.D. Research). Springer, Berlin

Luo X, Gu S, Lou Y, Xiong C, Chen B, Jin X (2018) Assessing the performance of GPS precise point positioning under different geomagnetic storm conditions during solar cycle 24. Sensors (basel, Switzerland) 18(6):1784. https://doi.org/10.3390/s18061784

Mannucci AJ, Tsurutani BT, Iijima BA, Komjathy A, Saito A, Gonzalez WD, Guarnierir FL, Kozyra JU, Skoug R (2005) Dayside global ionospheric responce to the major interplanetary events of October 29–30, 2003 "Halloween Storms". Geophys Res Lett 32(12):L12S02: https://doi.org/10.1029/2004GL021467

Mazher K, Tahir M, Ali K (2016) GNSS pseudorange smoothing: Linear vs non-linear filtering paradigm. In: 2016 IEEE aerospace conference. Big Sky, MT, pp 1–10. https://doi.org/10.1109/AERO.2016.7500779

Mengistu E, Damtie B, Moldwin MB, Nigussie M (2018) Comparison of GPS-TEC measurements with NeQuick2 and IRI model predictions in the low latitude East African region during varying solar activity period (1998 and 2008–2015). Adv Space Res 61(6):1456–1475. https://doi.org/10.1016/j.asr.2018.01.009

Mervart L, Lukes Z, Rocken C, Iwabuchi T (2008) Proceedings of the 21st international technical meeting of the satellite division of the institute of navigation (ION GNSS 2008), Savannah, GA, pp 397–405

Nava B, Radicella SM, Azpilicueta F (2011) Data ingestion into NeQuick 2. Radio Sci 46:RS0D17. https://doi.org/10.1029/2010RS004635

Park B, Lim C, Yun Y, Kim E, Kee C (2017) Optimal divergence-free Hatch filter for GNSS single-frequency measurement. Sensors 17(3):448

Peyret F, Bétaille D, Hintzy G (2000) High-precision application of GPS in the field of real-time equipment positioning. Autom Constr 9(3):299–314. https://doi.org/10.1016/S0926-5805(99)00058-8

Prange L, Orliac E, Dach R, Arnold D, Beutler G, Schaer S, Jäggi A (2017) CODE's five-system orbit and clock solution-the challenges of multi-GNSS data analysis. J Geod 91:345–360. https://doi.org/10.1007/s00190-016-0968-8

Rabbany AE (2002) Introduction to GPS: the global positioning system. Artech House, Norwood

Rizos C (2003) Trends in GPS technology and applications. In: 2nd international LBS workshop, Seoul, Korea

Seeber G (2003) Satellite geodesy, 2nd edn. Walter de Gruyter, Berlin

Shim JS et al (2011) CEDAR electrodynamics thermosphere ionosphere 1 (ETI). Challenge for systematic assessment of ionosphere/thermosphere models 1: NmF2, hmF2, and vertical drift using ground based observations. Space Weather 9:S12003. https://doi.org/10.1029/2011SW000727

Skone S (2001) The impact of magnetic storms on GPS receiver performance. J Geodesy 75:457–468. https://doi.org/10.1007/s001900100198

Suresh S, Dashora N (2016) Climatological response of Indian low-latitude ionosphere to geomagnetic storms. J Geophys Res Space Phys 121:4880–4897. https://doi.org/10.1002/2015JA022004

Teunissen PJG, Khodabandeh A (2015) Review and principles of PPP-RTK methods. J Geod 89:217. https://doi.org/10.1007/s00190-014-0771-3

Tian A, Dong D, Ning D, Fu C (2013) GPS single point positioning algorithm based on least squares. In: Sixth international symposium on computational intelligence and design, Hangzhou, pp 16–19. https://doi.org/10.1109/ISCID.2013.119

Venkatesh K, Fagundes PR, Seemala GK, de Jesus R, de Abreu AJ, Pillat VG (2014) On the performance of the IRI-2012 and NeQuick2 models during the increasing phase of the unusual 24th solar cycle in the Brazilian equatorial and low-latitude sectors. J Geophys Res Space Phys 119:5087–5105. https://doi.org/10.1002/2014JA019960

Wang M, Chai H, Li Y (2017) Performance analysis of BDS/GPS precise point positioning with undifferenced ambiguity resolution. Adv Space Res 60(12):2581–2595. https://doi.org/10.1016/j.asr.2017.01.045

Wang L, Li Z, Ge M, Neitzel F, Wang Z, Yuan H (2018) Validation and assessment of multi-GNSS real-time precise point positioning in simulated kinematic mode using IGS real-time service. Remote Sens 10(2):337. https://doi.org/10.3390/rs10020337

Warnant R, Kutiev I, Marinov P, Bavier M, Lejeune S (2007) Ionospheric and geomagnetic conditions during periods of degraded GPS position accuracy: 2. RTK events during disturbed and quiet geomagnetic conditions. Adv Space Res 39:881–888. https://doi.org/10.1016/j.asr.2006.06.018

Yousuf M, Dashora N, Sridhar M, Dutta G (2023) Long-term impact of ionospheric scintillations on kinematic precise point positioning: seasonal and solar activity dependence over Indian low latitudes. GPS Solut 27(1):40. https://doi.org/10.1007/s10291-022-01378-1

Zehentner N, Mayer-Gürr T (2016) Precise orbit determination based on raw GPS measurements. J Geod 90:275. https://doi.org/10.1007/s00190-015-0872-7

Zhao L, Li L, Zhao X (2009) An adaptive Hatch filter to minimize the effects of ionosphere and multipath for GPS single point positioning. In: International conference on mechatronics and automation, Changchun, pp 4167–4172. https://doi.org/10.1109/ICMA.2009.5246548